Eur. Phys. J. E (2015) **38**: 81
DOI 10.1140/epje/i2015-15081-8

THE EUROPEAN PHYSICAL JOURNAL E

Regular Article

Nematic phase characterisation of the self-assembling sphere-cylinders based on the theoretically calculated RDFs

Elena S. Pyanzina[1,a], Sofia S. Kantorovich[1,2], and Cristiano De Michele[3]

[1] Ural Federal University, Lenin av. 51, Ekaterinburg, 620000, Russia
[2] University of Vienna, Sensengasse 8, Vienna, 1090, Austria
[3] Dipartimento di Fisica, "Sapienza" Università di Roma, P.le Aldo Moro 5, 00185, Rome, Italy

Received 29 April 2015
Published online: 21 July 2015 –

Abstract. We put forward a theoretical framework to calculate pair distribution functions in the nematic liquid crystals formed by sphere-cylinders that self-assemble in linear chain structures. For a nematically ordered system, one can distinguish between the spatial correlations in the plane perpendicular to the crystalline axis, and in the direction parallel to the latter. Following this separation, we show that the RDFs in the parallel case can be described using a superposition of a chain model and Onsager distribution, whereas the RDFs in the perpendicular case turn out to be that of the soft disks. Based on this concept, we show how the spatial correlations in the system are influenced by the nematic order parameter. We conclude that even if the nematic ordering is high in the system, the imperfection of the crystal is strongly reflected in the pair distributions.

1 Introduction

Self-assembly-driven nematisation occurs when basic building blocks, due to anisotropic interactions, form linear semi-flexible aggregates, which may mutually align to form nematic liquid crystals (LCs) phases with macroscopic orientational ordered, if the concentration is sufficiently high. Many systems, such as rod-like micelles [1–3], fibers and fibrils [4–8], aqueous solutions of short (nano) [9,10] and long B-DNA [11–14], G-quadruplexes [15,16], chromonics [17–22] as well as cellulose nanocrystals [23], exhibit a self-assembly-driven transition from an isotropic to an orientationally ordered state on increasing concentration.

Recently, an Onsager-like theoretical approach has been proposed [24] to accurately describe the self-assembly-driven LC formation in the systems of anisotropic superquadrics with attractive patches. Since scattering experiments easily provide information on system structure in the form of structure factors, it is necessary to develop a formalism to theoretical calculations of density-density correlations based on the results of the predicted self-assembly and phase behaviour. In the case of the isotropic state, we put forward such an approach in ref. [25], where we used the analytically calculated radial distribution function (RDF) and its Fourier transform to predict the centre-centre structure factor. However, for the nematic phase, this approach is not applicable, as one needs to distinguish between the correlations along the nematic axis and those perpendicular to it.

In this paper we present a theoretical approach to calculate RDF of self-assembly-driven nematic LCs. We test the method against the same model system which has been already used in ref. [26], namely hard cylinders with attractive sites on their bases [27]. The latter model, and its variant where bent hard cylinders are employed, has also been used to study the physical properties of short DNA duplexes [28,29].

The paper is organised as follows. In the next section we describe the methods, both simulational (subsect. 2.1) and analytical. For the latter, we consider separately the aforementioned cases; namely we construct independently the RDFs parallel (subsect. 2.2) and perpendicular (subsect. 2.3) to the nematic axis. We extensively compare the analytical predictions to the results of computer simulations in sect. 3, also addressing separately the two situations. A summary of our work is provided in the Conclusion.

2 Methods: theory and simulations

2.1 Simulations

We performed canonical NVT Monte Carlo (MC) simulations of polymerising hard cylinders (HCs) with aspect ratio $X_0 = L/d = 2, 3$, where L and d are the length

[a] e-mail: elena.pyanzina@urfu.ru

Table 1. System parameters.

X_0	φ	α	M	d_{eff}	φ_{sd}	φ_{hd}
2	0.318	9.25	6.24	2.24	0.35	0.44
	0.380	12.03	6.10	2.18	0.46	0.55
	0.424	15.06	6.90	2.14	0.53	0.61
	0.470	18.95	8.54	2.11	0.61	0.68
3	0.318	13.75	6.67	2.16	0.35	0.43
	0.380	18.11	6.81	2.12	0.45	0.54
	0.424	21.75	7.61	2.10	0.50	0.60
	0.470	26.33	9.41	2.08	0.57	0.65

and diameter of HCs, respectively. MC simulations have been carried out in a cubic box with periodic boundary conditions. Reversible polymerisation occurs via end-to-end stacking due to the two attractive square-well sites placed on the two bases of the HCs. We studied 4 different fully nematic state points, with different temperature and concentration, for each elongation. The two attractive square-well sites are located along the long axis of the HC at a distance $L/2 + 0.15d/2$ from its centre of mass and sites belonging to distinct particles interact via the square-well (SW) potential, *i.e.* $\beta u_{\text{SW}} = -\beta u_0$, if $r < \delta$ and $\beta u_{\text{SW}} = 0$, if $r > \delta$, where r is the distance between the interacting sites, $\delta = 0.25d$ is the interaction range (*i.e.* the diameter of the attractive sites), βu_0 is the ratio between the binding energy and the thermal energy k_BT where k_B is the Boltzmann constant. L is the unit of length and temperature T^* will be given in reduced units of u_0/k_B. The position of the attractive sites and the range of the square-well interaction have been chosen in order to have a persistence length and a bonding volume compatible with values used in a recent study of DNA duplexes self-assembly [24]. Note that the effective length of the cylinders is actually defined by the position of the RDF first pick (in parallel case), which in turn sets the effective volume fraction.

The parameters used in the simulations are described in the first two columns (the semiaxis ratios X_0, and the volume fractions φ) of table 1. The directional character of the interactions favours the formation of chain aggregates, whose equilibrium distribution can be measured in simulations as well as calculated analytically [24]. These chains, if long enough, contribute to the isotropic-nematic transition when the volume fraction of the cylinders grows. In the third and fourth columns we provide the theoretical values for the average chain length M and the nematic parameter α. The remaining three columns of table 1 will be described later.

The main question we would like to address in this paper is how the nematic ordering influences the interparticle spatial correlations, which is why, in fig. 1, we present four simulation snapshots for the volume fraction 0.318 (left) and 0.47 (right). The semiaxis ratios are $X_0 = 2$ (upper row) and $X_0 = 3$ (lower row).

It is clearly seen that the nematic ordering increases with growing volume fraction and semiaxis ratio. This

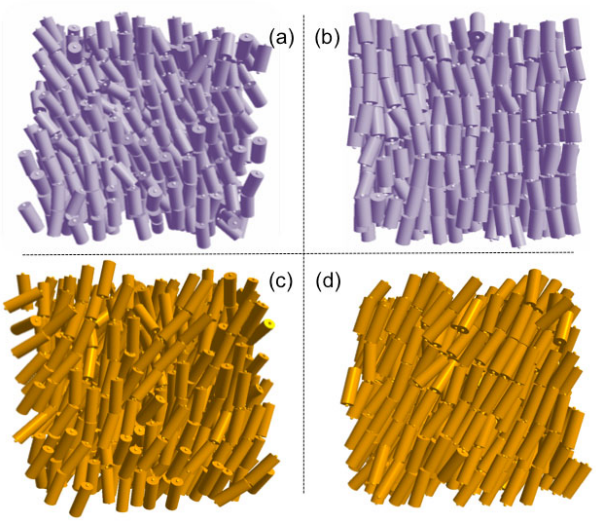

Fig. 1. Simulation snapshots for $X_0 = 2$ at (a) $\varphi = 0.318$, $T = 0.13$ and (b) $\varphi = 0.47$, $T = 0.12$ and for $X_0 = 3$ at (c) $\varphi = 0.318$, $T = 0.13$ and (d) $\varphi = 0.47$, $T = 0.12$.

influences the structural units observed in the cross-sections parallel and perpendicular to the nematic axis. For a perfect nematic order, one would expect to have only chain contributions parallel to the nematic axis, and ideal hard discs in the plane perpendicular to the nematic axis.

Let us check how accurate this assumption is for the systems under study and, in that case, what ways exist to handle the deviations.

2.2 Parallel case

The naive assumption for the RDF in the direction parallel to the nematic axis is that the distances within the chains would provide the major contribution to the spatial correlations. However, it would have been the only contribution, had all chains been perfectly aligned with the nematic axis. In reality, we know that the probability distribution function for a cylinder to be inclined by the angle θ from the nematic axes has the form proposed by Onsager [30]:

$$f_{\text{Ons}}(\theta) = \frac{1}{\sinh \alpha} \cosh(\alpha \cos \theta), \tag{2.1}$$

where α is the nematic parameter and θ is the angle between the particle and the nematic axis (see fig. 2(a)). From the geometry of the system $\theta = \arcsin(d/r)$. Thus the distribution function in our case is

$$f_{\text{Ons}}(r, \alpha) = \frac{1}{\sinh \alpha} \cosh\left(\alpha \sqrt{1 - \left(\frac{d}{r}\right)^2}\right). \tag{2.2}$$

Thus, to properly describe the RDF, one needs to use a superposition of the RDF of chains [24,25,31] and that of eq. (2.2). Earlier, in the isotropic case, we also used the superposition of the two effects to describe the RDF [25],

$$g_{\parallel}(r,T,X_0,\varphi,\alpha,\Delta)=\begin{cases} f_{\mathrm{Ons}}(r,\alpha), & \text{if } 0<r<L_{\mathrm{eff}}-\Delta;\\ \cdots & \\ f_{\mathrm{Ons}}(r,\alpha)+p^s/A_s(X_0,\varphi,\Delta), & \text{if } s\ L_{\mathrm{eff}}-\Delta\le r\le s\ L_{\mathrm{eff}}+\Delta;\\ f_{\mathrm{Ons}}(r,\alpha), & \text{if } s\ L_{\mathrm{eff}}+\Delta<r<(s+1)\ L_{\mathrm{eff}}-\Delta;\\ \cdots & \end{cases} \tag{2.3}$$

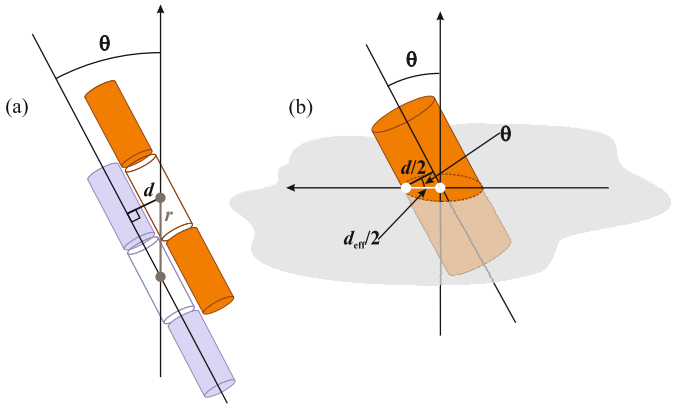

Fig. 2. Sketch of the chains in the nematic phase. (a) In the plane parallel to the nematic axis: the distance r between the centres of the cylinders depends on the nematic parameter through angle θ. (b) In the plane perpendicular to the nematic axis: the effective diameter d_{eff} changes depending on the nematic order parameter.

but there the contribution from the various contact distances of the elongated particles had to be taken into account. In the nematic phase instead, this contribution can be neglected, due to the fact that configurations, other than almost parallel ones, are not possible.

see eq. (2.3) *above*

Here, r is interparticle centre-centre distance,

$$p(T,X_0,\varphi)=\frac{M(T,X_0,\varphi)-1}{M(T,X_0,\varphi)}$$

is the probability to form a dimer (for details see [24]), $A_s(X_0,\varphi,\Delta)=s^3(L_{\mathrm{eff}}\Delta)^3\varphi/v_d$, where v_d is the volume of the particles and φ is the volume fraction, L_{eff} corresponds to the effective length of the particle.

The comparison of the prediction from eq. (2.3) and the results of the simulations will be provided in subsect. 3.1.

2.3 Perpendicular case

In the plane perpendicular to the nematic axis, one can assume the RDF to be approximately that of simple hard disks. However, as it is shown in fig. 2(b), the cross-section of the inclined cylinder has an elliptic rather than circular shape. On the other hand, the probability density distribution corresponding to eq. (2.1) is symmetric with respect to zero, which means that the average cross-section would be a circle with a certain effective diameter larger than d. In this manuscript, we will compare the simulation results obtained for the cylinders in the perpendicular case to two different RDFs: theoretical pair distribution taken from the work of Yuste and Santos [32,33]; and the simple Molecular Dynamics simulation for soft disks performed in the software package ESPResSo [34]. The main idea to calculate the RDF for hard disks put forward in works [32,33] is to combine RDF's for one and three dimensional systems:

$$\begin{aligned} g_{\perp}(r,\varphi) &= a(\varphi)g_{\mathrm{PY}}^{(1)}(r,\varphi\lambda^{(1)}(\varphi))\\ &\quad+[1-a(\varphi)]g_{\mathrm{PY}}^{(3)}(r,\varphi\lambda^{(3)}(\varphi)). \end{aligned} \tag{2.4}$$

Here, $g_{\mathrm{PY}}^{(k)}$ is RDF for k-dimensional hard spheres provided by the virial expansion up to first order of concentration, $a(\varphi)$ mixes the Percus-Yewick RDFs for hard rods and for hard spheres. The $\lambda^{(k)}(\varphi)$ scale the density of the reference systems (one and three dimensional). For any details see [32,33] and references therein. This formula is used for the disks of unit diameter, therefore we need to modify it. In the perpendicular case the effective diameter of the disk can be calculated as $d_{\mathrm{eff}}=d/\cos(\sqrt{2/\alpha})$ with the angle $\theta=\sqrt{2/\alpha}$ calculated on the basis of Onsager distribution (see, fig. 2(b)).

3 Results and discussions

3.1 Parallel case: how nematic is the "Nematic"?

In this section we investigate the influence of the semiaxis ratio and concentration of cylinders on the pair correlations. For this we use the systems described in table 1. The main question is how, with increasing concentration followed by the growth of the nematic order, the RDFs evolve, and if they converge to those of a perfect nematic, *i.e.* a nematic liquid crystal with all particles perfectly aligned. The answer is provided in figs. 3 and 4.

In fig. 3 we plot the RDFs calculated parallel to the nematic axis. In the left column the system of shorter cylinders $X_0=2$ is presented; in the right one we plot the results for the systems with $X_0=3$. The RDFs have obviously two main contributions: high peaks coming from the interparticle distances in chains and a constant slow drift to unity (for the distances not possible in chains), which is magnified in fig. 4 and is discussed a bit later in this section. Let us focus on chain peaks first. With growing volume fraction (from the top to the bottom of the figure), for both semiaxis ratios, the height of the peaks grows and their width slightly decreases. This is attributed to two effects: growing chain length and increasing value of α. Another interesting observation can be seen when

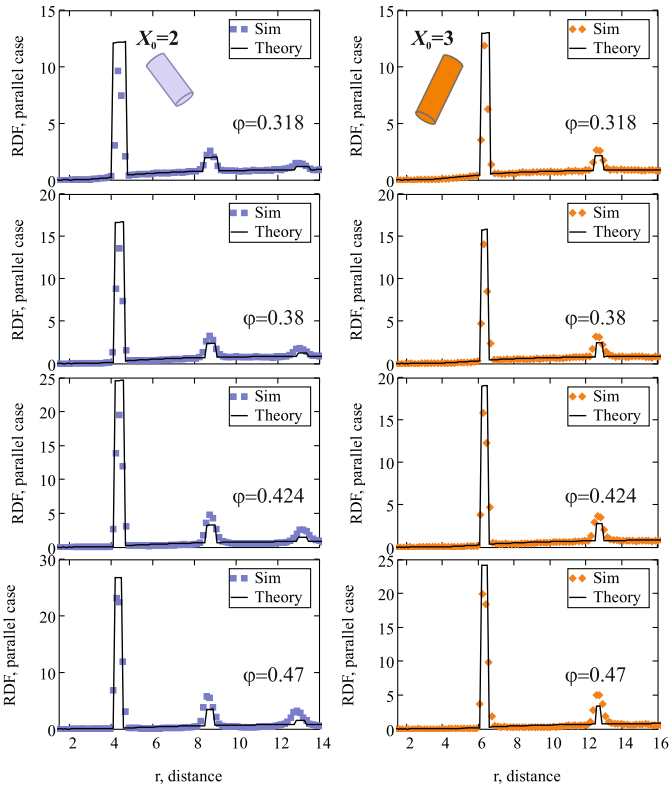

Fig. 3. Radial distribution functions parallel to the nematic axis as a function of the interparticle centre-centre distance. In the left column $X_0 = 2$, in the right one $X_0 = 3$. Volume fractions are given in the graphs. Simulation data are plotted with symbols; theoretical results are presented with solid lines. One can clearly see a contribution of chains in the form of well-pronounced peaks, and the impact of imperfect nematic alignment is reflected by the slow growth to unity.

comparing the RDFs for the same volume fraction but different values of X_0. Here, the width of the peaks is always smaller for $X_0 = 3$. One can understand this by considering the local rigidity of the chains and the contribution of the elongation to the growth of α (compare the values of the order parameter provided in table 1 for different X_0). The overall fluctuations along the chains made of long cylinders are weaker. Note that the peaks are lower for $X_0 = 3$, because the number density is smaller for this case, as the volume fractions are fixed.

In fig. 4 the zoomed version of RDFs is presented. We can clearly see that the drift mentioned above is very sensitive to the cylinder volume fraction. Thus the higher the value of φ, the lower the corresponding part of the RDFs, *i.e.* the slower the drift. In general, this drift shows the probability of finding the centres of two cylinders from different chains to lay on the same line (parallel to the nematic vector) at a given distance. For a perfect nematic this probability is zero for any distance; for a relatively disordered system with short chains one can expect the misalignment to be rather frequent. In other words, the slower the drift goes to unity, the lower the probability of such a misalignment to take place at shorter distances in the system. That is why this part of

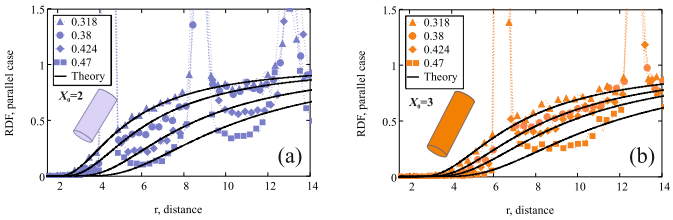

Fig. 4. Magnified plots of radial distribution functions parallel to the nematic axis as functions of the interparticle centre-centre distance. (a) $X_0 = 2$, (b) $X_0 = 3$. Volume fractions are given in the legend. Simulation data are plotted with symbols, theoretical results are presented with solid lines. It is evident that growing nematic order drives to a higher "drift" in the RDFs.

the RDF can be so well described by Onsager probability distributions. The other important observation, provided by the zoom, is that the peaks of the RDF are not exactly at the distances equal to $X_0 d$, but are regularly shifted towards larger r. This shift is related to the size of the attractive patch, and defines the effective height of the cylinders and rescales the overall volume fraction with the factor of approximately 8-10 per cent. This factor will play an important part in the perpendicular case.

In both plots one can see that the theoretical predictions agree very well with the simulation data. Thus, we can safely summarise the parallel case, confirming that even for high values of α the pair distributions are quite far from those expected for a perfect nematic ordering (chain peaks alternated with zero), which tells us that the imperfections of the ordering are in this case magnified in the RDFs.

3.2 Perpendicular case: soft disks

In the plane perpendicular to the nematic axis, the system can be thought of as one of disks. It would have been absolutely correct, had the system been perfectly nematic. In fig. 5, however it can be clearly seen that it is not the case. In this figure, analogously to the parallel case (see fig. 3), we plot RDFs for $X_0 = 2$ on the left and for $X_0 = 3$ on the right; the volume fraction grows from the top to the bottom. The RDFs for the cylinders are plotted with squares and rhombuses. In order to match the data with the analytical expression for hard disks (solid curves, eq. (2.4) [32,33]), we need to scale the hard-disk diameter and the area fraction of the latter. In order to check that the coincidence is not accidental, we perform the additional series of simulations, using Molecular Dynamics in ESPResSo [34] for soft disks and plot the results with dots.

At this point we can check that the scaling of the diameters and densities is physical. First of all, to match soft and hard disks, we calculate the effective diameter using the following expression:

$$d_{hd}^{\text{eff}} = \frac{\int_0^{R_c} \exp\left[-\beta U_{\text{WCA}}(x)\right] x^2 \mathrm{d}x}{\int_0^{R_c} \exp\left[-\beta U_{\text{WCA}}(x)\right] x \mathrm{d}x}, \qquad (3.1)$$

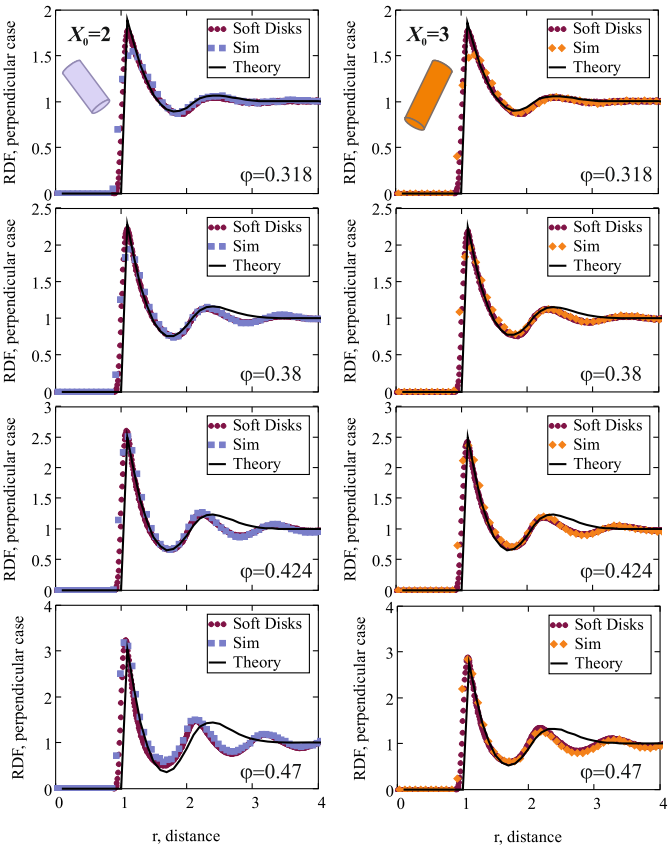

Fig. 5. Radial distribution functions perpendicular to the nematic axis as a function of the interparticle centre-centre distance. In the left column $X_0 = 2$, in the right one $X_0 = 3$. Volume fractions are given in the graphs. Simulation data for cylinders are plotted with symbols (pale violet squares and orange rhombuses, the effective area fraction and disk diameters are used), theoretical results (hard disks with effective area fraction and effective diameter) are presented with solid lines. The assumption of the disk model is confirmed by brown circles: Molecular Dynamics simulation results for soft disks with a corresponding area fraction.

with thermal energy $\beta = 1$ and Weeks-Chandler-Andersen potential for soft spheres (soft disks when used in 2D) [35] having the form

$$U_{\mathrm{WCA}}(r) = \begin{cases} 4\varepsilon\left[\left(\frac{\sigma}{r}\right)^{12} - \left(\frac{\sigma}{r}\right)^{6} + \frac{1}{4}\right], & \text{if } r \le 2^{\frac{1}{6}}\sigma, \\ 0, & \text{if } r \ge 2^{\frac{1}{6}}\sigma. \end{cases} \tag{3.2}$$

Here, we use $\varepsilon = 1$ and $\sigma = 1$. This value in our case is approximately 1.07. The next step is to evaluate the approximate area fraction of soft disks for the cylinders depending on the nematic order parameter α, using d_{eff}, the values of which are provided in table 1. Thus, we obtain the values of the $\varphi_{sd} = \varphi h_{\mathrm{eff}}/d_{\mathrm{eff}}$, where h_{eff} is the position of the parallel RDF first peak. Finally, the area fraction of the hard disks should be rescaled using $\varphi_{sd}(d_{hd}^{\mathrm{eff}})^2$. All values are provided in table 1.

The comparison works very well, and the system of cylinders indeed converges to that of soft disks in the plane perpendicular to the nematic vector with growing concentration, *i.e.* with increasing nematic parameter. Note that for the highest density, the analytical expression fails due to the limitations of the second-order expansion.

The main conclusion of this section is that even for high ordering, the spatial correlations are still far from the perfect case of hard disks; however, they can be effectively described by the RDFs of soft disks with proper scaling of the diameter and area fractions. The hard-disk pair correlation functions as expected agree well with the soft ones, immediately after the first peak. Finally, the influence of X_0 in this case is much less pronounced than in the parallel case.

4 Conclusion

In the present paper, we put forward a theoretical approach to calculate RDFs in the nematic LCs formed by sphere-cylinders, that self-assemble in linear chain structures. For a system with the nematic order, it is convenient to study spatial correlations in the plane perpendicular to the crystalline axis separately from those in the direction parallel to the latter. We used this split in our theoretical framework.

We found that the RDFs in the parallel case can be described using a superposition of a chain model and Onsager distribution. The width of the RDF's peaks due to chain formation is determined by the particle elongation. Namely, the higher the value of the cylinder semiaxis ratio, the more narrow the peaks. This is the consequence of the following: the chain formed by several highly elongated cylinders has the same metric length as the chain made of multiple short cylinders, as a result the chains made of long particles have less internal degrees of freedom. The background drift (slow increase of the RDF parts between the peaks) observed in the parallel case is caused by the imperfection of the nematic order. The drift is slower for a higher value of the nematic order parameter. The higher nematic order is provided by longer chains; however, in the longer chains the long-range ordering is also more pronounced. Thus, if two very long chains are even slightly inclined with respect to the nematic axis, the range of high probability to find two centres of the cylinders from different chains on the same line (parallel to the nematic vector) shifts towards larger distances.

The RDFs in the perpendicular case converge to that of the soft disks with growing nematic parameter. For the perfect nematic, the cross-section of the system of chains made of hard cylinders perpendicular to the nematic vector is made of perfect hard disks, whose diameter simply coincides with that of the cylinder. The inclination of chains leads to the effective increase of the disk diameter, which fluctuates, thus inducing an effective softness. We prove this by comparing the RDF obtained for hard cylinders (perpendicular case) to the RDF calculated in Molecular Dynamics simulations of soft disks and to the analytical pair correlation function of hard disks of an effective diameter, both with the corresponding area fractions.

In such a way, we elucidate how the spatial correlations in the system are influenced by the nematic order parameter and show that even if the nematic ordering is high, the imperfection of the liquid crystalline phase is strongly reflected in the pair distributions.

Our theoretical approach is rather general and as an input parameter uses only the semiaxis ratio, cylinders' volume fraction and the bonding free energy, which is why it is applicable to any system where the equilibrium self-assembly in chains causes the isotropic-nematic transition.

The research has been partially supported by Austrian Science Fund (FWF): START-Projekt Y 627-N27. S.S.K. is supported by the Ministry of Education and Science of the Russian Federation (Contract 02.A03.21.000, Project 3.2.2014/K). S.S.K. is grateful to the ETN-Colldense. E.S.P. was supported by the Grant of the President of the Russian Federation No MK-7131.2015.2 and RFBR grant mol-a 14-02-31746. S.S.K. and E.S.P. are grateful to the UrFU Stimulating Programme and were partially supported by mol-a-ved 15-32-20549. C.D.M. acknowledges support from MIUR-PRIN. The authors want to thank Michaela McCaffrey for linguistic suggestions.

References

1. A. Khan, Curr. Opin. Colloid Interface Sci. **1**, 614 (1996).
2. P. van der Schoot, M.E. Cates, Langmuir **10**, 670 (1994).
3. D.M. Kuntz, L.M. Walker, Soft Matter **4**, 286 (2008).
4. R. Mezzenga, J. Jung, J. Adamcik, Langmuir **26**, 10401 (2010).
5. Chiu Fan Lee, Phys. Rev. E **80**, 031902 (2009).
6. A. Ciferri, Liq. Cryst. **34**, 693 (2007).
7. A. Aggeli, M. Bell, L.M. Carrick, C.W.G. Fishwick, R. Harding, P.J. Mawer, S.E. Radford, A.E. Strong, N. Boden, J. Am. Chem. Soc. **125**, 9619 (2003).
8. H.-D. Dörfler, Adv. Colloid Interface Sci. **98**, 285 (2002).
9. M. Nakata, G. Zanchetta, B.D. Chapman, C.D. Jones, J.O. Cross, R. Pindak, T. Bellini, N.A. Clark, Science **318**, 1276 (2007).
10. C. Maffeo, B. Luan, A. Aksimentiev, Nucl. Acids Res. **40**, 3812 (2012).
11. C. Robinson, Tetrahedron **13**, 219 (1961).
12. F. Livolant, A.M. Levelut, J. Doucet, J.P. Benoit, Nature **339**, 724 (1989).
13. K. Merchant, R.L. Rill, Biophys. J. **73**, 3154 (1997).
14. F. Tombolato, A. Ferrarini, J. Chem. Phys. **122**, 054908 (2005).
15. N.B. Wilding, J. Phys.: Condens. Matter **9**, 585 (1996).
16. S. Bonazzi, M. Capobianco, M.M. De Morais, A. Garbesi, G. Gottarelli, M.G. Ponzi Bossi, G.P. Spada, L. Tondelli, J. Am. Chem. Soc. **113**, 5809 (1991).
17. H.-S. Park, S.-W. Kang, L. Tortora, Yu. Nastishin, D. Finotello, S. Kumar, O.D. Lavrentovich, J. Phys. Chem. B **112**, 16307 (2008).
18. F. Chami, M.R. Wilson, J. Am. Chem. Soc. **132**, 7794 (2010).
19. J. Lydon, Liq. Cryst. **38**, 1663 (2011).
20. P.K. Maiti, Y. Lansac, M.A. Glaser, N.A. Clark, Liq. Cryst. **29**, 619 (2002).
21. R.G. Edwards, J.R. Henderson, R.L. Pinning, Mol. Phys. **86**, 567 (1995).
22. J.R. Henderson, J. Chem. Phys. **113**, 5965 (2000).
23. J.P.F. Lagerwall, C. Schutz, M. Salajkova, J.-H.J.H. Noh, J.H. Park, G. Scalia, L. Bergstrom, NPG Asia Mater **6**, e80 (2014).
24. C. De Michele, T. Bellini, F. Sciortino, Macromolecules **45**, 1090 (2012).
25. S. Kantorovich, E. Pyanzina, C. De Michele, F. Sciortino, Soft Matter **9**, 4412 (2013).
26. K.T. Nguyen, F. Sciortino, C. De Michele, Langmuir **30**, 4814 (2014).
27. C. De Michele, J. Comput. Phys. **229**, 3276 (2010).
28. C. De Michele, L. Rovigatti, T. Bellini, F. Sciortino, Soft Matter **8**, 8388 (2012).
29. K.T. Nguyen, A. Battisti, D. Ancora, F. Sciortino, C. De Michele, Soft Matter **11**, 2934 (2015).
30. L. Onsager, Ann. N.Y. Acad. Sci. **51**, 627 (1949).
31. E. Pyanzina, S. Kantorovich, J.J. Cerda, A. Ivanov, C. Holm, Mol. Phys. **107**, 571 (2009).
32. S. Bravo Yuste, A. Santos, Phys. Rev. A **43**, 5418 (1991).
33. S. Bravo Yuste, A. Santos, J. Chem. Phys. **99**, 2020 (1993).
34. A. Arnold, O. Lenz, S. Kesselheim, R. Weeber, F. Fahrenberger, D. Roehm, P. Kosovan, C. Holm, in *Meshfree Methods for Partial Differential Equations VI*, edited by Michael Griebel, Marc Alexander Schweitzer, Vol. **89** of *Lecture Notes in Computational Science and Engineering* (Springer Berlin Heidelberg, 2013) pp. 1–23.
35. J.D. Weeks, D. Chandler, H.C. Andersen, J. Chem. Phys. **54**, 5237 (1971).